Article

Journal of
Nanoscience and Nanotechnology
Vol. 20, 6047–6056, 2020
www.aspbs.com/jnn

CeO_2–NiO Nanoflakes: Assessment and Their Anticancer Activity with HepG2 and MCF7 Cancer Cells

Suliman Yousef Al-Omar[1], Naushad Ahmad[2, 3, *], Ashfaq Ahmad[2], Manal A. Al-Fwuaires[4], and Manawwer Alam[2]

[1] *Doping Research Chair, Department of Zoology, College of Science, King Saud University, Riyadh-11451, Kingdom of Saudi Arabia*
[2] *Department of Chemistry, College of Science, King Saud University, Riyadh-11451, Kingdom of Saudi Arabia*
[3] *Central Laboratory, College of Science, King Saud University, Riyadh-11451, Kingdom of Saudi Arabia*
[4] *Department of Biological Sciences, Faculty of Science, King Faisal University, Hofuf-31982, Al-Ahsa, Kingdom of Saudi Arabia*

The present study describes the synthesis of CeO_2–NiO nanoflakes (CeNiO-NFs) via solution process in a very short time span and it was utilized for to control the growth against liver and breast cancer cells. The processed nanocomposites were characterized with several instruments such as of their physicochemical characteristics such as XRD, FT-IR, TGA/DTG/DSC, DLS, BET, SEM-EDX, TEM and UV-visible spectrophotometer respectively. The acquired results are in full justification with the physical data and it suggests that the formed CeO_2–NiO nanocomposite is in nanoflakes shaped (∼20–25 nm). Moreover, anticancer activity of CeNiO-NFs was investigated through MTT and NRU assays for liver (HepG2) and breast (MCF7) cancer cells. The results demonstrated that it exhibited dose-dependent cytotoxic effects in the range of 1–100 μg/mL and revealed a reduction in their cell viability in response from low and high concentration of CeNiO-NFs.

Keywords: Nanocomposite, Cancer Cell, Cytotoxicity, CeO_2, NiO, MTT, NRU.

1. INTRODUCTION

Millions of peoples are dying every year due to liver and breast cancer, regardless of many types of medications. These traumatic diseases and medicines also influences the major organs of the body by metabolic biological responses and serious side impacts with medicines. In recent years, shared approach of nanotechnology and biotechnology risen as a better alternative for the treatment of these diseases since a nanoscale medicate seem to be little side effects [1, 2]. Being smaller in size, nanoparticles (NPs) can be effortlessly enter to the cells, therefore, played a compelling part for the treatment of cancer. The nanoscale drugs have targeted action on cancer cells due to the large surface zone that facilitate the incorporation of high drug doses [1–3].

The nanostructured materials with controlled morphology, particle distribution, crystal structure, and porosity have shown increasing research interest due to broad scope of applications, promising results, and their unique physicochemical properties, which are significantly different than those of bulk materials [4–6]. Among the numerous types of NPs, which have biocidal properties are advantageous than conventional drugs due to the great resistance against cancer cells [7, 8]. Moreover, these are comparatively more economical and stable than the conventional antibiotics. Towards this direction, many types of nanoscale carriers such as dendrimers, polymeric micelles, and inorganic nanocomposites have been investigated and used as anticancer drugs, biosensing, gene delivery and cell imaging, in order to minimize the side effects and uncontrolled chain reaction in survival patients and enhance the antitumor drug efficacy target therapies [1–3, 9, 10]. Among various organic polymeric NPs, inorganic NPs of metal, metal oxides and its nanocomposites exhibit promising anticancer property, which have biocompatibility and minimized side effects in the body after the administration [11–13].

Many inorganic nano-scale materials such as nickel, cerium, copper, gadolinium, gold, magnetite, silver, zinc, titanium, iron oxide, nickel oxide, and cerium oxide have been synthesized with controlled factors through

*Author to whom correspondence should be addressed.

green, chemical and physical methods, more or less environmental-friendly, and widely used against the diseases [14–18]. Several reports concerning the NPs/composites of cerium and nickel with various morphological structures such as nanotubes, nanocubes, nanowires, nanorods, and nanopolyhedra are well documented in the literature [19–28]. Especially, nano-cerium oxide, owing to its biocompatibility, high isoelectric point, mechanical strength, and adsorption capability, is having attractive and wide applications such as sensing and catalytic reactions in liquids and gas medium [29]. Furthermore, due to the high surface-to-volume ratio (s/v), oxygen storage capacity and oxygen ion conductivity, it has a high adsorption capacity for sugars, enzymes, toxic pollutants, proteins, and amino acids [30, 31]. Nano-nickel oxide is a product with many unused characteristics, which include a high level of surface energy and high surface area. Cytotoxic impacts in leukemia cancer cells, apoptosis in mouse epidermal JB6 cells, and natural potential risk related to their harmfulness are categorically well detailed in articles [22, 23].

The shown work reports the bi-metallic oxide of two oxides (CeO_2 and NiO) as a cerium nickel oxide nanocomposite (CeNiO-NFs) for the examination of anticancer activity against liver (HepG2) and breast (MCF7) cancer cells lines. The structural, morphological, optical, porosity and thermal properties of CeNiO-NFs have been determined by physical and chemical characterization based on X-ray diffraction pattern (XRD), transmission electron microscopy (TEM), scanning electron microscopy equipped with energy dispersive X-ray analysis (SEM-EDX), UV-Vis spectrophotometry, dynamic light scattering (DLS), Brunauer-Emmett-Teller (BET), Thermogravimetric analysis and Differential scanning calorimetry (TGA/DSC).

2. MATERIALS AND METHODS

2.1. Materials

Cerium nitrate hexahydrate ($Ce(NO_3)_3 \cdot 6H_2O$), Nickel nitrate hexahydrate ($Ni(NO_3)_2 \cdot 6H_2O$), and glycine ($C_2H_5NO_2$) were purchased from Sigma-Aldrich chemical corp. and used without any further modification. 3-(4,5-dimethylthiazol-2-yl)-2,5-diphenyl tetrazolium bromide) which is formally known as MTT assay and neutral red dye (NRU) were procured from sigma and stored in the dark condition. Dulbecco's Modified Eagle Medium (DMEM) cell medium, fetal bovine serum (FBS), trypsin-EDTA and antibiotics/antimycotic solution were procured from Invitogen. All other reagents and solvents were of analytical grades.

2.2. Synthesis of CeO_2–NiO Nanoflakes (CeNiO-NFs)

CeNiO-NFs were synthesized by the solution method. Briefly, equimolar aqueous solution of $Ce(NO_3)_3 \cdot 6H_2O$ and $Ni(NO_3)_2 \cdot 6H_2O$ (0.1 M) were mixed into a 250 mL round bottle flask, under constant stirring condition. Then 100 mL of glycine (0.4 M) was dropped into the mixture. The pH was adjusted to 8–9 by using liquid ammonia ($NH_3 \cdot H_2O$) and was heated at 353 K on hot plate for 3 h. After refluxing, the obtained precipitate was sequentially washed with deionized ultrapure water, ethyl alcohol and acetone, and dried at room temperature. Thereafter, the obtained black powder was annealed at 300 °C for 2 h at a ramp rate of 5 °C min^{-1}, and characterized for the morphology, structure and composition.

2.3. Characterizations of CeO_2–NiO Nanoflakes (CeNiO-NFs)

The crystallinity and phases of the powder sample was analyzed by X-ray powder diffractometer (XRD, Ultima IV, Rigaku, Japan) with $Cu_{K\alpha}$ radiation (0.154178 nm) in range of 10–80° with 6° min^{-1} scanning speed. The chemical functional characteristic was measured by Fourier-transform infrared (FT-IR, Perkin Elmer spectrometer 4100) using the KBr pellet technique at room temperature. The thermal decompositions were performed by using Mettler Toledo TGA/DSC1STARe thermal analyzer, Switzerland, between 50–900 °C at the heating ramp of 20 °C min^{-1} in nitrogen flow (20 mL min^{-1}). The optical and band gap (E_g) energy was measured through UV-vis absorption spectroscopy (Shimadzu UV-2450 spectrophotometer, Japan). Hydrodynamic particle size, polydispersity index (PDI) and Zeta potential in an aqueous medium was determined by dynamic light scattering (DLS) analyzer (Zeta-Sizer-HT Malvern instrument, UK) at 25 °C. BET surface area was measured on a Micromeritics TriStar 3000 BET Analyzer, taking a value of 0.162 nm^2 for the cross-sectional area of the N_2 molecule adsorbed at 77 K. TEM were obtained using a JEOL 2010 microscope operating at an accelerating voltage of 80 kV. The purity of nanocomposite material/elemental composition was analyzed with the use of EDS, equipped with the provision of SEM at room temperature (JEOL, JED-2200 series, Japan).

2.4. Anticancer Activity

Human liver (HepG2) and breast (MCF7) cancer cell lines were cultured in DMEM medium supplemented with 10% FBS and 1% antibiotic-antimycotic solution. Both cell lines were maintained at 37 °C in 5% CO_2 humid atmosphere. The relative cytotoxicity/cell viability of synthesized CeNiO-NFs was evaluated against both cancer cells with MTT and NRU assays [32, 33]. In brief, 1×10^4 cells/well were plated in 96-well plates and allowed to adhere in a CO_2 incubator at 37 °C for overnight. After overnight incubation, cells were exposed at different concentration of CeNiO-NFs (1–100 μg/mL) for 24 h. After the respective treatment, 10 μL MTT (5 μg/mL) was added in each well and incubated additionally 4 h. At the end of the reaction, supernatant was discarded

from all wells and DMSO (200 μL) were added in each well and mixed to homogenize. The plates were kept on rocker shaker for 10 min at room temperature and then absorbance of plates was measured at 570 nm by using a multiwall microplate reader (Synergy-HT, BioTek). The non-treated cells were used as control. The values were compared with control sets, run under identical conditions without fabricated nanocomposites. Similarly, cytotoxicity of sample was performed by NRU assay. In brief, after overnight incubation, 10×10^4 cells were treated with different concentration of CeNiO-NFs (1–100 μg/ml) for 24 h. After the treatment, the medium was washed off with PBS and further incubated for 3 h in a medium containing 50 μg/mL neutral red dye. Then, medium was taken out and wells were washed with a solution (0.5% formaldehyde and 1% calcium chloride). Plates were then incubated to extract the dye at 37 °C for 20 min in a mixture of 1% acetic acid and 50% ethanol. The plates were read at 550 nm using multiwell microplate reader. The morphology changes of treated cells were observed under the phase contrast inverted microscope and cell images were grabbed at 20×.

3. RESULTS AND DISCUSSION

3.1. XRD Analysis

To investigate the structural and phase properties, the product was characterized by XRD pattern. Figure 1 exhibited the XRD of synthesized CeNiO-NFs annealed at 300 °C for 2 h. From the obtained spectrum, there is no unidentified peaks like $Ce(OH)_2$ and $Ni(OH)_2$ was found in the diffraction pattern, validated the purity and complete transformation into composite material. The powder material showed a mixed diffraction reflections of CeO_2 (JCPDS 75-8371) and NiO (JCPDS 01-1239). The face centered cubic phase CeO_2 is revealed by the diffraction peaks at positions of 28.4°, 33.4°, 47.2°, 56.9°, 69.6°, and 76.4° corresponding to (111), (200), (220), (311), (400), and (331) planes, respectively. Similarly, by addition of nickel content in the samples, a series of peaks were observed at positions of 37.1°, 43.9°, 62.7°, which correspond to (111), (200), and (220) crystal planes, respectively, indicate the formation of cubic phase of NiO.

3.2. FT-IR Analysis

To confirm the chemical compositions, the synthesized nanocomposite was characterized via FT-IR spectroscopy at room-temperature in range of 400–4000 cm^{-1}. The obtained spectrum is represented as Figure 2. As per the obtained spectrum, various well-defined peaks at 3438, 2496, 2365, 2206, 1619, 1460, 1065, 867, 775, 702, 475 cm^{-1} were observed. The peak centered at 3438 and 1619 cm^{-1} is attributable to the O–H stretching and bending vibrations mode of absorbed water molecules, respectively [34]. The peak observed at 1460 and 1065 cm^{-1} is assigned the stretching vibration mode of C–O originating

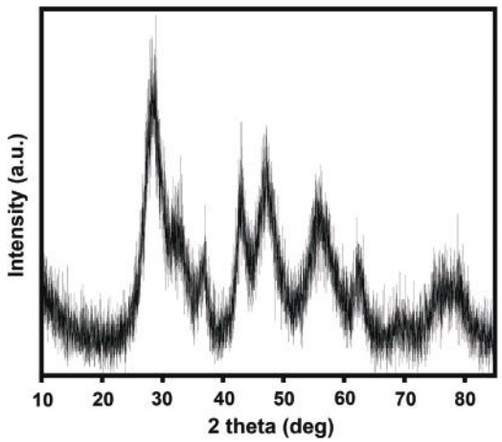

Figure 1. The X-ray powder diffraction patterns of prepared CeNiO-NFs.

from the adsorption of atmospheric CO_2 or ethanol, adsorb from the environment due to its high surface-to-volume ratio [35]. Appearance of two very small peaks at 1381 and 881 cm^{-1} reflect the nitrate group [34]. The characteristic sharp and strong absorption in a range of 500–700 cm^{-1} ascribing to vibration of CeO_2 bond in the CeNiO-NFs. The band appears at 475 cm^{-1} is related to the stretching vibration of cubic NiO structure [36]. Any other band related to impurities has not been detected in this spectrum, which again confirms that the processed material is pure.

3.3. Thermal Analysis

In order to reveal the heat treatment of nanocomposite, TG-DTG and DSC analyses were carried out in nitrogen atmosphere (Fig. 3). It is readily seen that the TGA curve showed two steps of weight loss in a temperature range of 50–300 °C and 300–600 °C, respectively, also confirmed via DTG and DSC curves. The first weight loss can assign

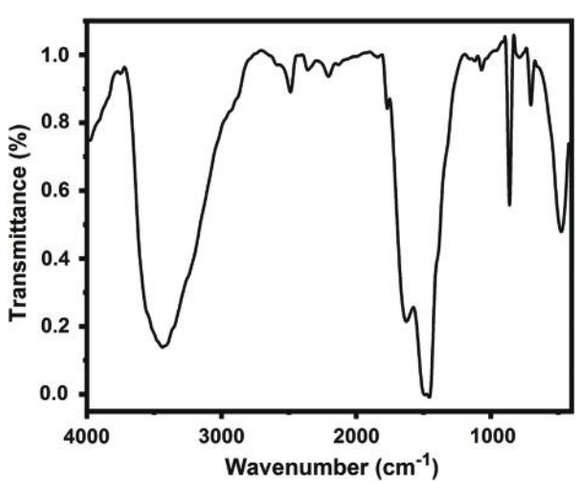

Figure 2. FT-IR spectrum of CeNiO-NFs.

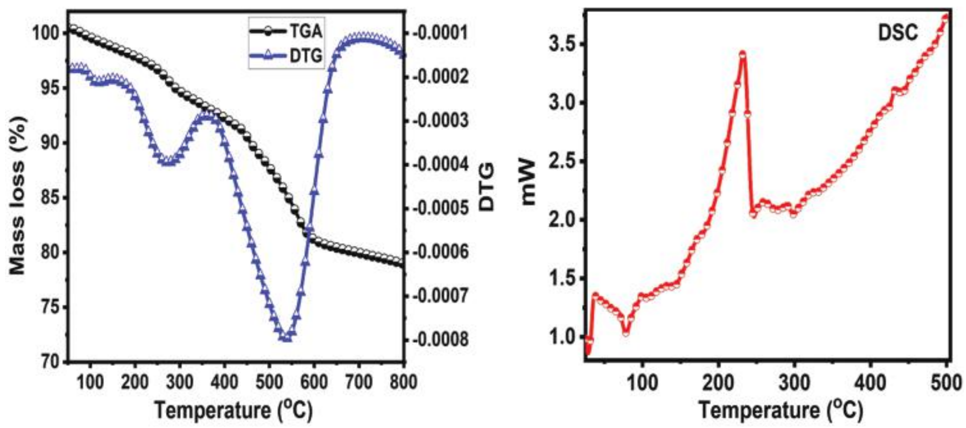

Figure 3. TG-DTG-DSC decomposition curves of CeNiO-NFs.

the evaporation of water molecule (HOH) whereas the second weight loss is associated with the thermal decomposition of hydroxides of Ce and Ni. When temperature rose above 600 °C, TGA/DSC data shows the steady mode, which again confirms the thermal stability of the processed material and indicates the complete and stable formation of CeNiO-NFs.

3.4. UV-Vis Spectrophotometer Analysis

The UV-Vis spectrophotometer was utilized to know the optical absorption of formed CeNiO-NFs analyzed in the range of 200–800 nm wavelength and spectrum is illustrated as Figure 4. From the obtained data, it realizes that a well-defined absorption band at 295 nm and are optically and photocatalytically active [37]. The absorption coefficient (α) and band gap energy (E_g) can be written as $(\alpha h\upsilon)^n \propto h\upsilon\text{-}E_g$, where υ is the frequency, h is Planck's constant, and n is either 2 for a direct transition or 1/2 for an indirect transition [38]. The direct band gap energy for CeNiO-NCs can be estimated by the plot of $(\alpha h\upsilon)^2$ versus photon energy ($h\upsilon$), as shown Figure 4(b). As a result, the value of band gap energy is 4.20 eV for the CeNiO-NFs sample [38]. The UV spectrum showed a well-defined peak and not related to any other peaks which again confirm that the synthesized NPs are pure nanocomposite (CeNiO-NCs).

3.5. Dynamic Light Scattering (DLS) Analysis

DLS analysis was used to find out the hydrodynamic size, polydispersity index (PDI) and surface zeta potential of the synthesized NFs in an aqueous environment, results are shown in Figure 5. The hydrodynamic particles size distribution was observed between 200–400 nm and the average size was observed ∼292 nm (Fig. 5(a)), whereas the Zeta potential was estimated to be +39 mV (Fig. 5(b)). The PDI value of NFs was 0.849. As evident that the PDI value '0' represents monodisperse distribution whereas value '1' represents polydisperse distribution [39]. The obtained results suggested that it have a tendency to agglomerate in an aqueous state. The NFs size was differed from TEM due to the particles agglomeration.

3.6. Porosity Measurement

The Porosity parameters were investigated by nitrogen adsorption/desorption measurements and presented

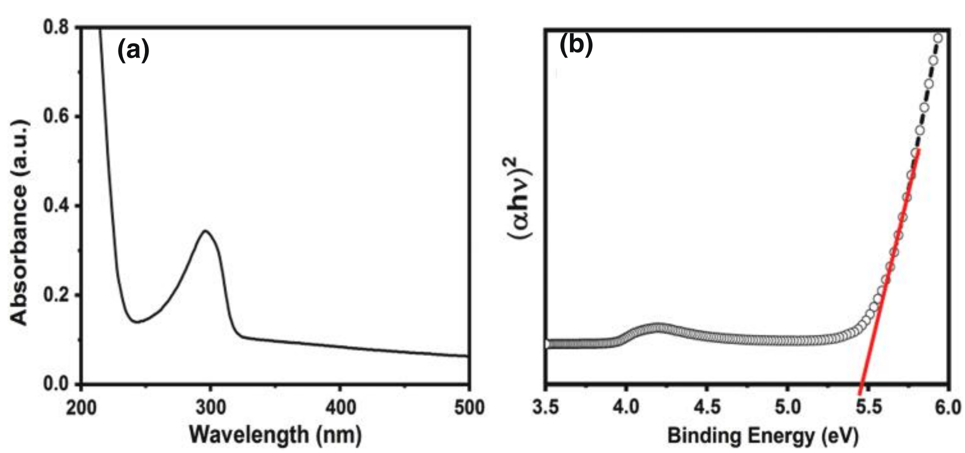

Figure 4. UV-vis absorption spectra (a and b) band gap energy of CeNiO-NFs.

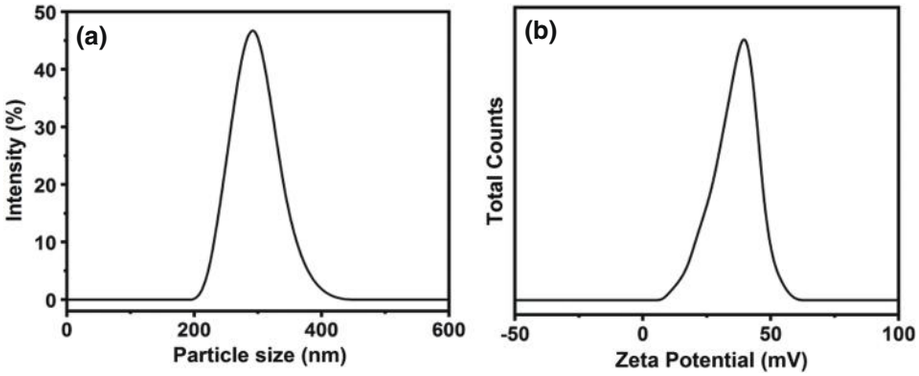

Figure 5. Hydrodynamic size (a) and zeta potential analyses (b) of CeNiO-NFs.

in Figure 6. The BET surface area, pore size distribution, and pore volume were 104.56 m^2/g, 11.88 nm, and 0.296 cm^3/g, respectively. The isotherm can be classified as type IV according to the profile of a hysteresis loop in the high relative pressure (P/P_0) range between 0.7–1.0. This reveals that the as-prepared NFs has a typical mesoporous structure, which is further verified from the BJH pore size distribution (PSD), shown in Figure 6(b). The PSD result demonstrated that synthesized porous CeNiO-NFs had multiple pore sizes, major pore size at 7 nm with other minors at 5.5, and 13 nm. This result indicates that it had good surface area with pore size distribution that was advantageous for the diffusion, transportation and contact of NCs in cancer cell lines.

3.7. Morphological and Elemental Compositional Analysis

The size, morphology and composition aspects of the sample were characterized by SEM-EDX and TEM. The SEM analysis with EDX of the CeNiO-NFs is presented in Figures 7(a) and (b), respectively. It is observed that the particles are made of many bunches of NFs and grown in very high density with in nanoscale range (size ∼20–25 nm). To determine the elemental composition, the prepared NFs were examined via EDX equipped with SEM. As shown in EDX spectrum (Fig. 7(b)), only well-defined peaks of Ce, Ni and O elements were seen and no other element was detected which confirm that synthesized NCs are composed of these three elements. Further the atomic percentage of cerium and nickel was found 33% and 66%, respectively. The % composition of element NFs provides evidence of reduced binary metal oxides and it's in accord with the results obtained from XRD.

Through TEM observation, it reveals that the CeNiO-NFs is mainly poised of non-spherical hexagonal shape and are often agglomerated into small aggregates which indicates the successful incorporation of NiO onto CeO_2, illustrated in Figure 8. The average diameter calculated from TEM images was found to be ∼20–25 nm. Numerous NFs consist of pore structure which may benefit the transport of analytes and also provide more catalytic sites.

3.8. Cytotoxicity Evaluation

3.8.1. Cytotoxic Activity of CeNiO-NCs by MTT Assay

Cytotoxicity test of a nanomaterial is the first-level evaluation before biomedical applications. The MTT assay was employed to estimate the cytotoxic effect of CeNiO-NFs on HepG2 and MCF7 cells. The results of cytotoxicity assessments are summarized in Figure 9. HepG2 and MCF7 cells were interacted at altered concentrations

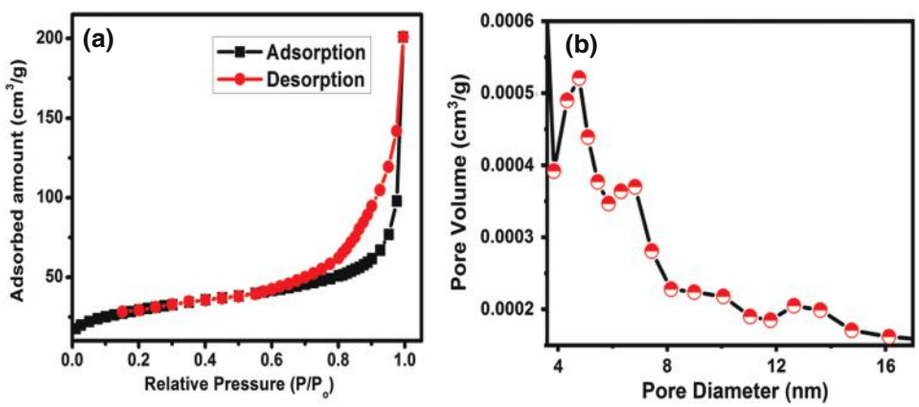

Figure 6. (a) N_2 adsorption–desorption isotherm and (b) pore-size distribution curve of CeNiO-NFs.

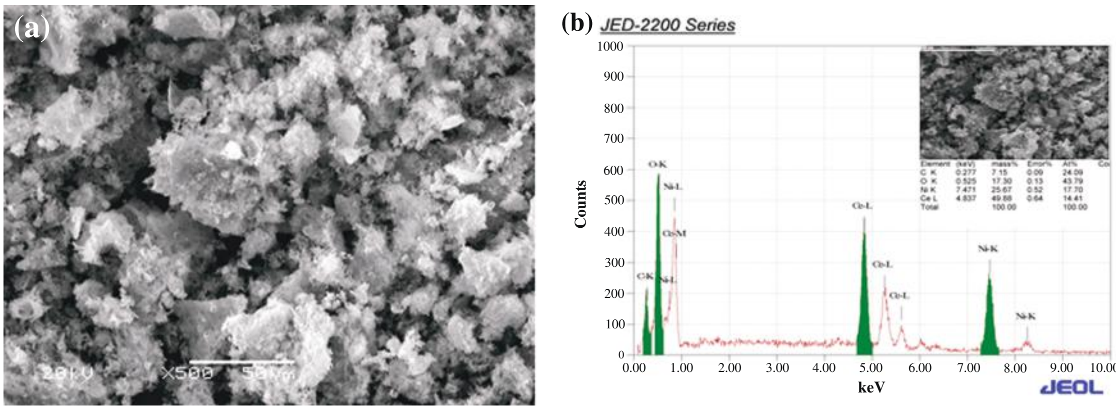

Figure 7. SEM-EDS images of the synthesized CeNiO-NFs (a) nanoflakes and (b) EDS spectra.

(1–100 μg/mL) of CeNiO-NFs for 24 h. The received data's exposed CeNiO-NFs induced a concentration relayent and it reduces the viability of cell of HepG2 and MCF7 cell lines. The cells at 25 μg/mL and enhanced conc were initiate to be cytotoxic and promote the lethality of cells. However, the cells reacted at 10 μg/mL and lower conc were observed to be non-cytotoxic. The % cell viability was recorded as 80, 59 and 47% in HepG2 cells at 25, 50 and 100 μg/mL of CeNiO-NCs, respectively (Fig. 9(a)). Whereas, the percent cell viability was recorded as 87, 76 and 60% in MCF7 cells at 25, 50 and 100 μg/mL of CeNiO-NCs, respectively (Fig. 9(b)). From the analysis, it was found that at 10 μg/mL and lower concentrations of CeNiO-NFs did not show any significant cytotoxicity in both the cell lines, suggesting a dose-dependent effect.

3.8.2. Cytotoxic Assessment by NRU Assay

The toxicity response with CeNiO-NFs in HepG2 and MCF7 cells also scrutinize through neutral red uptake assay (NRU). The obtained results are summarized in Figure 10. HepG2 and MCF7 cells exposed to 1–100 μg/mL of CeNiO-NFs for 24 h also showed a concentration-dependent and found to be decreased in the cell viability. The CeNiO-NFs exposed to HepG2 and MCF7 cells at 25 and above concentrations were found to be cytotoxic. The cell viability drops at 25, 50 and 100 μg/ml of CeNiO-NFs was verified as 83, 54 and 51% in HepG2 cells (Fig. 10(a)) and 84, 74 and 52% in MCF7 cells (Fig. 10(b)), respectively. As similar to MTT assay, the CeNiO-NFs at 10 μg/mL and lower conc not represent any note-worthy reduction in the cell viability of both cells.

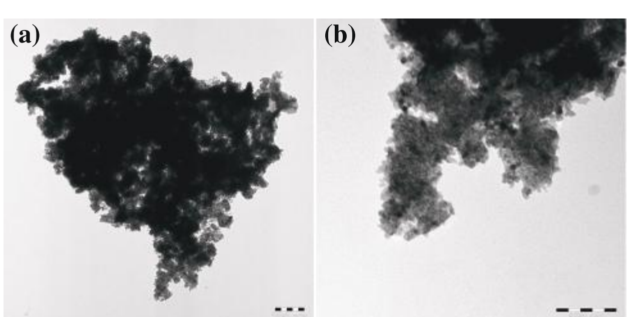

Figure 8. TEM images of the synthesized CeNiO-NFs (a) low and (b) high magnification.

3.8.3. Morphological Studies of Control and Treated Cells

The alterations in the cells morphology was observed and given in Figures 11 and 12. A concentration dependent morphological change in HepG2 and MCF7 cells were observed after the interaction of CeNiO-NFs. HepG2 and MCF7 cells exposed to 25, 50 and 100 μg/mL conc of CeNiO-NFs loses their pure shape and cell connection aptitude as compared to the control.

3.9. Discussion

With the advancement and increased development in the area of nanotechnology, produces the enormous amount of different shaped nanostructures either via physical, chemical or other methods [40]. Among a series of nanomaterials, the oxide nanostructured materials exhibit larger applications in various fields [41]. The metal oxides nanostructures, which have larger surface area, high reactivity and small size in the form of different shaped nanostructures such as nanoparticles, nanotubes, nanobelts, nanowires etc. are widely being used as commercial products in the form of sun screen lotion, cosmetics, food products, medicines, textiles etc. [42]. Due to the small size and organized morphology, the nano structures can have the possibility to reach easily and affect different human body organs such as lung, liver, kidney, brain, spleen, heart etc. through inhalation and absorption process [43]. In the present work the prepared NCs in the form of NFs shaped structures exhibit special morphology with high density, which easily enter in to the cells structures from any side and have capability to interact to the cells organelles (DNA, RNA, ribosomes, endoplasmic reticulum etc.) [44]. It postulates that these foreign NCs material interaction with cells generated ROS (reactive oxygen species) in the cells which are responsible for the cell death. The ROS

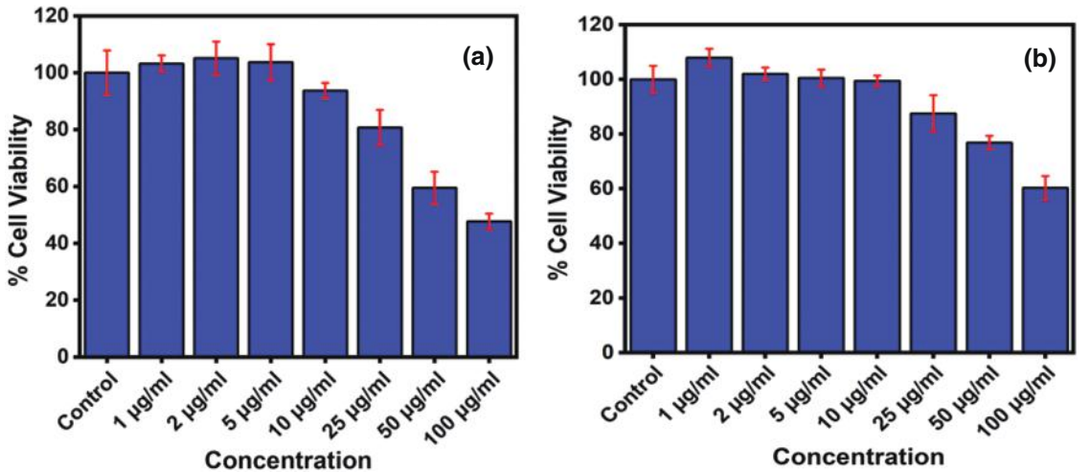

Figure 9. Effect of concentration of CeNiO-NFs on the cell viability of (a) HepG2 and (b) MCF7 cancer cell line by MTT assay.

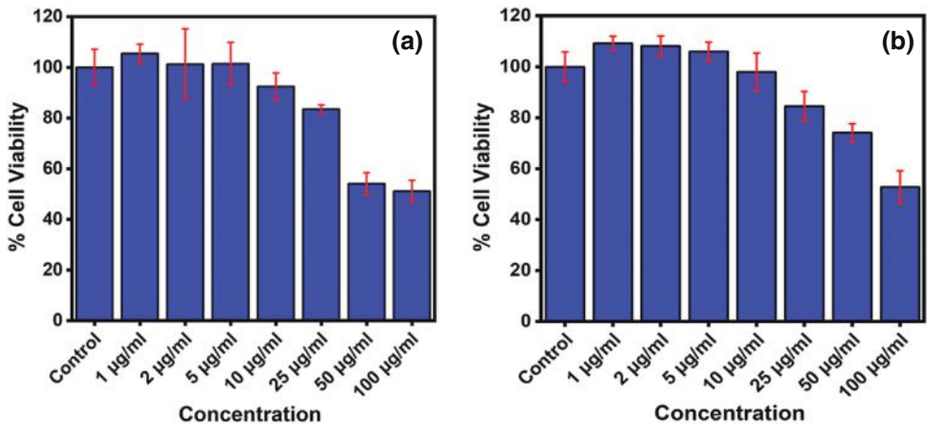

Figure 10. Effect of concentration of CeNiO-NFs on the cell viability of (a) HepG2 and (b) MCF7 cancer cell lines by NRU assay.

have possibility to disturb the function of cells through acting of cell components (DNA, protein, lipids etc.) which leads to cell death [45]. In the present study planned with aim to investigate the potential cytotoxic responses of liver (HepG2) and breast (MCF7) cancer cells with interaction of prepared NCs. For this, we have opted the well-known MTT and NRU assays for the assessment of cytotoxicity with prepared nanostructures in 24 h incubation period. From the obtained results it revealed that a substantial dose dependent cytotoxicity in cells was happened. At low conc/dose the cells were not much affected may be due to the NFs morphology and density whereas when the doses of structures were increased in the cells, the cells death was much affected [46]. We may also assume that the cells death (HepG2 and MCF7) was also affected with used preparation method, size and geometry of the nanostructure [47]. The mechanism and causes behind the cells death and their biochemical behavior study needs detailed investigations which are under progress.

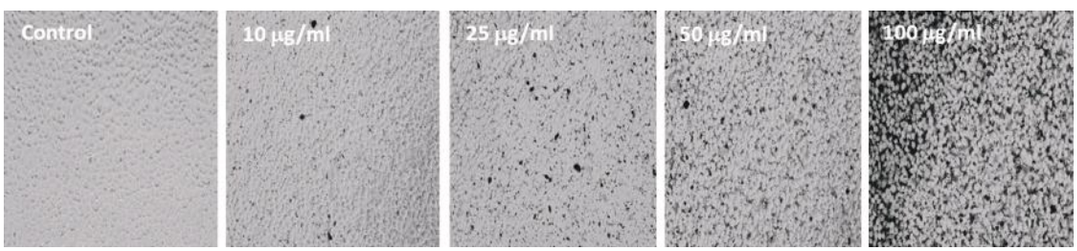

Figure 11. Morphological changes in HepG2 cells exposed to different concentrations of CeNiO-NFs for 24 h.

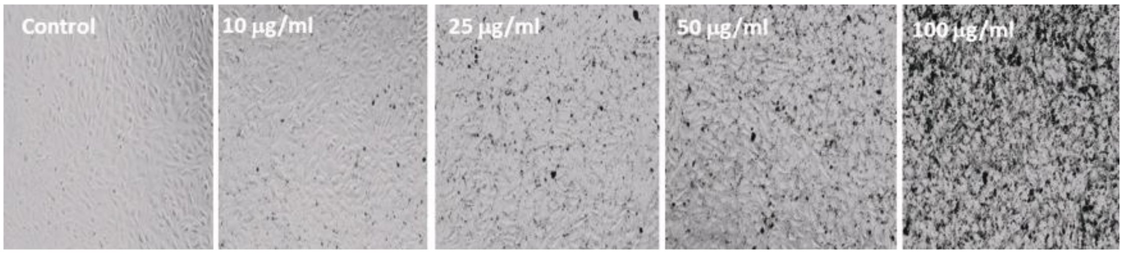

Figure 12. Morphological changes in MCF7 cells exposed to different concentrations of CeNiO-NFs for 24 h.

4. CONCLUSIONS

The summary of the present work demonstrates that the composite of cerium and nickel (CeNiO-NFs) was prepared via solution combustion process in a very short time span. Further the composite was annealed to get highly crystalline nanostructure. For this various characterizations tools were used to check their physical and chemicals parameters such as X-ray diffraction pattern was used to known their size and crystalline nature of the processed material. The general morphology of the processed material was accessed through SEM and TEM, which confirms that the prepared nanocomposite size is about ~20–25 nm, flakes in shape. The chemical finger print of the processed NCs analyzed through FT-IR spectroscopy, which also denotes that it does not show any residues and additive in the material except pure material. The optical property material was measured via UV-vis spectroscopy which showed the peak at 295 nm and band gap 4.20 eV, which show the material is optically active. The DLS and Zeta potential are the significant analysis in aqueous medium, which gives the polydisparity, hydrodynamic particles size distribution was ~292 nm with zeta estimated to be +39 mV. Including this, the BET surface area, pore size distribution, and pore volume were 104.56 m^2/g, 11.88 nm, and 0.296 cm^3/g, respectively were again confirm that the prepared material exhibit good porosity with a very small diameter. The present anticancer study validates that the treatments with prepared NCs in the form of NFs against liver (HepG2) and breast (MCF7) cancer cells affected with dose dependent concentration of NFs. The cell death or % viability was evaluated with MTT and NRU assays, which reveals that a sequential change was observed from low to high doses of nanostructures. At low concentrations the cell death was not much affected whereas when the doses of nanostructures were increased death in cells were much affected. The significant of the present work is to evaluate the anticancer property of the processed material. Although several parameters were required for theto understand the anticancer property of the prepared material but at initially it realizes that the overall implementation of the functional concentration of nanostructures material is very significant for the initiation and promotion as an anticancer drug.

Acknowledgments: This project was supported by the Researchers Supporting Project number (RSP-2019/35), King Saud University, Riyadh, Saudi Arabia.

References and Notes

1. Wong, K.K.Y. and Liu, X.L., **2012**. Nano medicine: A primer for surgeons. *Pediatric Surgery International, 28*, pp.943–951, DOI: 10.1007/s00383-012-3162-y.
2. Xu, Z.P., Zeng, Q.H., Lu, G.Q. and Yu, A.B., **2006**. Inorganic nanoparticles as carriers for efficient cellular delivery. *Chemical Engineering Science, 61*, pp.1027–1040, DOI: 10.1016/j.ces.2005.06.019.
3. Saleem, M.N., Munusamy, P., Ranjan, A., Alqublan, H., Pickrell, G. and Nammalwar, S., **2009**. Silica-antibiotic hybrid nanoparticles for targeting intracellular pathogens. *Antimicrobial Agents and Chemotherapy, 53*, pp.4270–4274, DOI: 10.1128/AAC.00815-09.
4. Kuang, D.B., Lei, B.X., Pan, Y.P., Yu, X.Y. and Su, C.Y., **2009**. Fabrication of novel hierar-chical β-Ni$(OH)_2$ and NiO microspheres via an easy hydrothermal process. *Journal of Physical Chemistry, 113*(4), pp.5508–5513.
5. Guo, M.N., Guo, C.X., Jin, L.Y., Wang, Y.J., Lu, J.Q. and Luo, M.F., **2010**. Nano-sized CeO_2 with extra-high surface area and its activity for CO oxidation. *Materials Letters, 64*(14), pp.1638–1640.
6. Gurunathan, S., Kalishwaralal, K., Vaidyanathan, R., Deepak, V., Pandian, S.R.K., Muniyandi, J., Hariharan, N. and Eom, S.H., **2009**. Biosynthesis, purification and characterization of silver nanoparticles using *Escherichia coli*. *Colloids and Surfaces B, 74*(1), pp.328–335.
7. Xiang, J.Y., Tu, J.P., Zhang, L., Zhou, Y., Wang, X.L. and Shi, S.J., **2010**. Self-assembled synthesis of hierarchical nanostructured CuO with various morphologies and their application as anodes for lithium ion batteries. *Journal of Power Sources, 195*(1), pp.313–319.
8. Xiang, J.Y., Tu, J.P., Zhang, L., Zhou, Y., Wang, X.L. and Shi, S.J., **2010**. Simple synthesis of surface-modified hierarchical copper oxide spheres with needle-like morphology as anode for lithium ion batteries. *Electrochimica Acta, 55*, p.1820, DOI: 10.1016/j.electacta.2009.10.073.
9. Wang, J.Q., Sui, M.H. and Fan, W.M., **2010**. Nanoparticles for tumor targeted therapies and their pharmaco kinetics. *Current Drug Metabolism, 11*, pp.129–141, DOI: 10.2174/138920010791110827.
10. Liu, Z., Tabakman, S., Welsher, K. and Dai, H.J., **2009**. Carbon nanotubes in biology and medicine: *In vitro* and *in vivo* detection, imaging, and drug deliver. *Nano Research, 2*, pp.85–120, DOI: 10.1007/s12274-009-9009-8.
11. Wang, L., Liu, Y., Li, W., Jiang, X., Ji, Y., Wu, X., Xu, L., Qiu, Y., Zhao, K., Wei, T., Li, Y., Zhao, Y. and Chen, C., **2011**. Selective targeting of gold nanorods at the mitochondria of cancer cells: Implications for cancer therapy. *Nano Letters, 11*, pp.772–780, DOI: 10.1021/nl103992v.
12. Doria, G., Conde, J., Veigas, B., Giestas, L., Almeida, C., Assunçao, M., Rosa, J. and Baptista, P.V., **2012**. Noble metal nanoparticles for bio sensing applications. *Sensors, 12*, pp.1657–1687, DOI: 10. 3390/s120201657.

13. Wang, A.Z., Langer, R. and Farokhzad, O.C., **2012**. Nanoparticle delivery of cancer drugs. *Annual Review of Medicine, 63*, pp.185–198, DOI: 10. 1146/annurev-med-040210-162544.

14. Engelbrekt, C., Malcho, P., Andersen, J., Zhang, L., Stahl, K., Li, B., Hu, J. and Zhang, J., **2014**. Selective synthesis of clinoatacamite $Cu_2(OH)_3Cl$ and tenorite CuO nanoparticles by pH control. *Journal of Nanoparticle Research, 16*, pp.25–56.

15. Yang, S. and Gao, L., **2006**. Controlled synthesis and self-assembly of CeO_2 nanocubes. *Journal of the American Chemical Society, 128*(29), pp.9330–9331.

16. Iravani, S., Korbekandi, H., Mirmohammadi, S.V. and Zolfaghari, B., **2014**. Synthesis of silver nanoparticles: Chemical, physical and biological methods. *Research in Pharmaceutical Sciences, 9*, pp.385–406.

17. Mittal, A.K., Chisti, Y. and Banerjee, U.C., **2013**. Synthesis of metallic nanoparticles using plant extracts. *Biotechnology Advances, 31*, pp.346–356, DOI: 10.1016/j.biotechadv.2013.01.003.

18. Noruzi, M., Zare, D., Khoshnevisan, K. and Davoodi, D., **2011**. Rapid green synthesis of gold nanoparticles using Rosa hybrida petal extract at room temperature. *Spectrochimica Acta, 79*, pp.1461–1465, DOI: 10.1016/j.saa.2011.05.001.

19. Kumar, S., Kim, G.W., Koo, B.H., Sharma, S.K., Knobel, M. and Lee, C.G., **2011**. Structural and magnetic study of a dilute magnetic semiconductor: Fe doped CeO_2 nanoparticles. *Journal of Nanoscience and Nanotechnology, 11*, pp.555–559, DOI: 10.1166/jnn.2011.3176.

20. Michel, C.R. and Preciado, A.H.M., **2014**. CO sensor based on thick films of 3D hierarchical CeO_2 architectures. *Sensors and Actuators, B, 197*, pp.177–184, DOI: 10.1016/j.snb.2014.02.090.

21. Meng, F. and Wang, L., **2013**. Hydrothermal synthesis of monocrystalline CeO_2 nanopoles and their room temperature ferromagnetism. *Materials Letters, 100*(1), pp.86–88.

22. Ipas, C., Andreescu, D., Patel, A., Goia, D., Andreescu, S. and Wallace, K.N., **2009**. Toxicity and developmental defects of different sizes and shape nickel nanoparticles in zebrafish. *Environmental Science and Technology, 43*, pp.6349–6356, DOI: 10.1021/es9010543.

23. Zhao, J., Bowman, L., Zhang, X., Shi, X., Jiang, B., Castranova, V. and Ding, M., **2009**. Metallic nickel nano and fine particles induce JB6 cell apoptosis through a caspase-8/AIF mediated cytochrome c-independent pathway. *Journal of Nanobiotechnology, 7*(2), p.13, DOI: 10.1186/1477-3155-7-2.

24. Liu, B., Li, Q., Du, X., Liu, B., Yao, M., Li, Z., Liu, R., Liu, D., Zou, X., Lv, H., Li, D., Zou, B., Cui, T. and Zou, G., **2011**. Facile hydrothermal synthesis of CeO_2 nanosheets with high reactive exposure surface. *Journal of Alloys and Compounds, 509*, pp.6720–6724, DOI: 10.1016/j.jallcom.2011.03.156.

25. Guo, D., Wu, C., Li, X., Jiang, H., Wang, X. and Chen, B., **2008**. In vitro cellular uptake and cytotoxic effect of functionalized nickel nanoparticles on leukemia cancer cells. *Journal of Nanoscience and Nanotechnology, 8*, pp.2301–2307, DOI: 10.1166/jnn.2008.311.

26. Rao, R., Yang, M., Ling, Q., Zhang, Q., Liu, H., Zhang, A. and Chen, W., **2013**. Mesoporous CeO_2 nanobelts synthesized by a facile hydrothermal route via controlling cationic type and concentration of alkali. *Microporous and Mesoporous Materials, 169*, pp.81–87, DOI: 10.1016/j.micromeso.2012.10.021.

27. Jha, S.K., Kumar, C.N., Raj, R.P., Jha, N.S. and Mohan, S., **2014**. Synthesis of 3D porous CeO_2/reduced graphene oxide xerogel composite and low level detection of H_2O_2. *Electrochimica Acta, 120*, pp.308–313, DOI: 10.1016/j.electacta.2013.12.051.

28. Anupriya, K., Vivek, E. and Subramanian, B., **2014**. Facile synthesis of ceria nanoparticles by precipitation route for UV blockers. *Journal of Alloys and Compounds, 590*, pp.406–410, DOI: 10.1016/j.jallcom.2013.12.121.

29. Mehta, A., Patil, S., Bang, H., Cho, H.J. and Seal, S., **2007**. A novel multivalent nanomaterial based hydrogen peroxide sensor. *Sensors and Actuators, A, 134*, pp.146–151, DOI: 10.1016/j.sna.2006.05.028.

30. Meng, F.M., Wang, L.N. and Cui, J.B., **2013**. Controllable synthesis and optical properties of nano-CeO_2 via a facile hydrothermal route. *Journal of Alloys and Compounds, 556*, pp.102–108, DOI: 10.1016/j.jallcom.2012.12.096.

31. Primo, A., Marino, T., Corma, A., Molinari, R. and García, H., **2011**. Efficient visible-light photocatalytic water splitting by minute amounts of gold supported on nanoparticulate CeO_2 obtained by a biopolymer templating method. *Journal of the American Chemical Society, 133*, pp.6930–6933, DOI: 10.1021/ja2011498.

32. Siddiqui, M.A., Singh, G., Kashyap, M.P., Khanna, V.K., Yadav, S., Chandra, D. and Pant, A.B., **2008**. Influence of cytotoxic doses of 4-hydroxynonenal on selected neuro transmitter receptors in PC-12 cells. *Toxicology in Vitro, 22*(7), pp.1681–1688.

33. Siddiqui, M.A., Kashyap, M.P., Kumar, V., Al-Khedhairy, A.A., Musarrat, J. and Pant, A.B., **2010**. Protective potential of trans-resveratrol against 4-hydroxynonenal induced damage in PC12 cells. *Toxicology in Vitro, 24*(6), pp.1592–1598.

34. Chauhan, M.S., Kumar, R., Umar, A., Chauhan, S., Kumar, G., Hwang, S.W. and Al-Hajry, A., **2011**. Utilization of ZnO nanocones for photocatalytic degradation of Acridine orange. *Journal of Nanoscience and Nanotechnology, 11*, pp.4061–4066, DOI: 10.1166/jnn.2011.4166.

35. Chu, X. and Zhang, H., **2009**. Catalytic decomposition of formaldehyde on nanometer manganese dioxide. *Modern Applied Science, 3*, pp.177–181.

36. Ni, X., Zhao, Q., Li, B., Cheng, J. and Zheng, H., **2006**. Interconnected β-$Ni(OH)_2$ sheets and their morphology-retained transformation into mesostructured Ni. *Solid State Communications, 137*(11), pp.585–588.

37. Khan, S.B., Faisal, M., Rahman, M.M. and Jamal, A., **2011**. Exploration of CeO_2 nano particles as a chemi-sensor and photocatalyst for environmental applications. *Science of the Total Environment, 409*, pp.2987–2992, DOI: 10.1016/j.scitotenv.2011.04.019.

38. Li, X., Li, J., Huo, D., Xiu, Z. and Sun, X., **2009**. Facile synthesis under near-atmospheric conditions and physicochemical properties of hairy CeO_2 nanocrystallines. *The Journal of Physical Chemistry C, 113*, pp.1806–1811.

39. Wahab, R., Khan, F. and Al-Khedhairy, A.A., **2018**. Hematite iron oxide nanoparticles: Apoptosis of myoblast cancer cells and their arithmetical assessment, *RSC Advances, 8*, pp.24750–24759.

40. Ahmad, J., Wahab, R., Siddiqui, M.A., Musarrat, J. and Al-Khedhairy, A.A., **2015**. Zinc oxide quantum dots: A potential candidate to detain liver cancer cells. *Bioprocess and Biosystems Engineering, 38*(1), pp.155–163.

41. Wahab, R., Siddiqui, M.A., Saquib, Q., Dwivedi, S., Ahmad, J., Musarrat, J., Al-Khedhairy, A.A. and Shin, H.S., **2014**. ZnO nanoparticles induced oxidative stress and apoptosis in HepG2 and MCF7 cancer cells and their antibacterial activity. *Colloids and Surfaces B: Biointerfaces, 117*, pp.267–276, DOI: 10.1016/j.colsurfb.2014.02.038.

42. Siddiqui, M.A., Saquib, Q., Ahamed, M., Farshori, N.N., Ahmad, J., Wahab, R., Khan, S.T., Alhadlaq, H.A., Musarrat, J., Al-Khedhairy, A.A. and Pant, A.B., **2015**. Molybdenum nano particles-induced cytotoxicity, oxidative stress, G2/M arrest, and DNA damage in mouse skin fibroblast cells (L929). *Colloids and Surfaces B: Biointerfaces, 125*, pp.73–81. DOI: 10.1016/j.colsurfb.2014.11.014.

43. Bahadar, H., Maqbool, F., Niaz, K. and Abdollahi, M., **2016**. Toxicity of nanoparticles and an overview of current experimental models. *Iranian Biomedical Journal, 20*(1), pp.1–11.

44. Wahab, R., Yang, Y.B., Umar, A., Singh, S., Hwang, I.H., Shin, H.S. and Kim, Y.S., **2012**. Platinum quantum dots and their cytotoxic effect towards myoblast cancer cells (C2C12). *Journal of Biomedical Nanotechnology, 8*(3), pp.424–431, DOI: 10.1166/jbn.2012.1448.

45. Zhang, Y., Bai, Y., Jia, J., Gao, N., Li, Y., Zhang, R., Jiang, G. and Yan, B., **2014**. Perturbation of physiological systems by nanoparticles. *Chemical Society Reviews, 43*(10), pp.3762–3809.

46. Arasu, M.V., Madankumar, A., Theerthagiri, J., Salla, S., Prabu, S., Kim, H.S., Al-Dhabi, N.A., Arokiyaraj, S. and Duraipandiyan, V., **2019**. Synthesis and characterization of ZnO nanoflakes anchored carbon nanoplates for antioxidant and anticancer activity in MCF7 cell lines. *Materials Science and Engineering: C, 102*, pp.536–540, DOI: 10. 1016/j.msec.2019.04.068.

47. Jarosz, A., Skoda, M., Dudek, I. and Szukiewicz, D., **2016**. Oxidative stress and mito chondrial activation as the main mechanisms underlying graphene toxicity against human cancer cells. *Oxidative Medicine and Cellular Longevity, 2016*, Article ID 5851035.

Received: 27 October 2019. Accepted: 18 December 2019.